A Simplified Method for Calculating the Crack-Tip Field of Functionally Graded Materials Using the Domain Integral

P. Gu[1]

M. Dao
Assoc. Mem. ASME

R. J. Asaro

Division of Structural Engineering,
University of California at San Diego,
La Jolla, CA 92093-0085

A finite element based method is proposed for calculating stress intensity factors of functionally graded materials (FGMs). We show that the standard domain integral is sufficiently accurate when applied to FGMs; the nonhomogeneous term in the domain integral for nonhomogeneous materials is very small compared to the first term (the standard domain integral). In order to obtain it, the domain integral is evaluated around the crack tip using sufficiently fine mesh. We have estimated the error in neglecting the second term in terms of the radius of the domain for the domain integration, the material properties and their gradients. The advantage of the proposed method is that, besides its accuracy, it does not require the input of material gradients, derivatives of material properties; and existing finite element codes can be used for FGMs without much additional work. The numerical examples show that it is accurate and efficient. Also, a discussion on the fracture of the FGM interlayer structure is given.

1 Introduction

The mechanics of functionally graded materials (FGM), including crack problems, have been intensively studied recently. It has been shown that for FGM crack problems the crack tip has a regular square-root singularity, the stress and displacement near-tip fields are of the same forms as those for homogeneous materials (see Delale and Erdogan, 1983, 1988; Gu and Asaro, 1997a, b). So the influence of material gradients at the near tip manifests itself through the stress intensity factors. In other words, the stress intensity factors uniquely characterize the near-tip field. Knowing the structure of the crack-tip field, it is important to accurately calculate the stress intensity factors and determine the effect of material gradients on them for different geometries and loadings, including those often-used specimens. Finite element analysis which can handle difficult material behaviors and geometries as well as various loadings provides useful and the most often-used way to solve mechanical and thermal problems including those involving FGMs. In this paper, we present a simple and sufficiently accurate finite element method for calculating the crack-tip field for FGMs, which can be easily incorporated into existing finite element codes and commercial software packages without much additional work.

The often-used method to calculate the crack-tip field, stress intensity factors (elastic case), and energy release rate (elastic or plastic case), involves evaluating the J-integral (Rice, 1968) using the solved stress and deformation fields around crack tip. For homogeneous materials, this has been an efficient way since the path independence of the J-integral allows us to perform the calculation along a path not too close to the tip so that the inaccuracy of field variables at the tip region due to the singularity can be avoided. Later, the domain integral method has been developed to perform the calculation of the J-integral (Li, Shih and Needleman, 1985; Shih, Moran and Nakamura, 1986; Moran and Shih, 1987). The domain integral method has been shown to be more efficient and more accurate than direct calculation of the J-integral, since the domain integration comes more naturally than the line integration of the two-dimensional space and the surface integration of the three dimensional space in finite element analysis. Works along similar line as the domain integral can be found in the early papers by Parks (1974, 1977), Hellen (1975) and deLorenzi (1982), whose virtual crack extension method is the special case of the domain integral. The domain integral method has been implemented in numerous programs to solve crack mechanics, including the well-known commercial package ABAQUS. In this paper, we use the domain integral methodology to treat the FGM case. In the non-homogeneous case, there is an additional term besides the regular one due to the variation of material properties. In our analysis of two-dimensional elastic crack problems of non-homogeneous materials, to capture the singularity and material property variation, the mesh is designed such that the smallest elements at the crack tip are very small, about 10^{-5} times a characteristic length, which is usually the crack length, and even much smaller for inelastic problems. The material variation is achieved by using corresponding material properties at Gauss integration points (different Gauss points have different properties). For such mesh design, to perform the domain integration, the domains can be chosen as the circular regions formed by the first few rings of elements. In such a situation, we show that the second term in the domain integral for nonhomogeneity is very small compared to the first term, the standard domain integral, and may be neglected. Therefore the domain integral can be calculated numerically in the same way as that for homogeneous materials, using the standard domain integral. From the numerical point of view, this allows us to apply existing finite element programs for homogeneous materials to nonhomogeneous materials, avoiding the additional programming work.

The current study is focused on elastic two-dimensional and three-dimensional problems. The method may also be extended

[1] MARC Analysis Research Corporation, 4330 La Jolla Village Drive, Suite 320, San Diego, CA 92122.

Contributed by the Applied Mechanics Division of THE AMERICAN SOCIETY OF MECHANICAL ENGINEERS for publication in the ASME JOURNAL OF APPLIED MECHANICS.

Discussion on the paper should be addressed to the Technical Editor, Professor Lewis T. Wheeler, Department of Mechanical Engineering, University of Houston, Houston, TX 77204-4792, and will be accepted until four months after final publication of the paper itself in the ASME JOURNAL OF APPLIED MECHANICS.

Manuscript received by the ASME Applied Mechanics Division, Mar. 9, 1998; final revision, July 14, 1998. Associate Technical Editor: M.-J. Pindera.

to the nonlinear material behavior. The numerical examples given include a sandwiched structure with a FGM interlayer, which illustrates the advantage of using FGM to reduce material mismatch between the upper and lower layers. For such structures, cracks may form at one side and propagate to the other side through the FGM interlayer when the microscopic defects and external loading are favorable. The crack in the sandwiched structure solved in this paper is along the layers' thickness direction with the crack tip inside the FGM, and the loading includes remote bending, three-point bending, and four-point bending. This kind of configuration may also be good for fracture testing of FGMs since the FGMs are usually very thin so that mechanical testing may be handled when bonding them to two bulk materials. In general, the solutions to the three-point bending and four-point bending specimens depend on several parameters, including geometry, loading, and material variation. We write them in a compact form such that the functionality of each parameter may be clearly understood. These examples show a way to systemically present the solutions so that they can be documented and are easy to use in practice.

The paper consists of three sections. Besides this Introduction, Section 2 is the discussion of the domain integral method in which we estimate the second term due to nonhomogeneity and show that based on the analysis, the term can be neglected. Section 3 contains numerical examples.

2 Numerical Method

The crack-tip stress field in a FGM has a regular singularity (see Delale and Erdogan, 1983, 1988; Gu and Asaro, 1997a, b) and the singular term for plane problems is given by

$$\sigma_{ij} = \frac{K_I}{\sqrt{2\pi r}} \sigma_{ij}^I(\theta) + \frac{K_{II}}{\sqrt{2\pi r}} \sigma_{ij}^{II}(\theta) \tag{1}$$

where the angular functions σ_{ij}^I and σ_{ij}^{II} are independent of material properties and their variations and are the same as those for homogeneous materials. The displacement singular term is given by

$$u_i = \frac{K_I}{2\mu_0}\sqrt{\frac{r}{2\pi}}\, u_i^I(\theta) + \frac{K_{II}}{2\mu_0}\sqrt{\frac{r}{2\pi}}\, u_i^{II}(\theta). \tag{2}$$

Here, μ_0 is the shear modulus at the crack tip. The angular functions u_i^I and u_i^{II} are also independent of material gradients, and are the same as those for homogeneous materials. Material gradients only affect the near-tip fields through the mode I and mode II stress intensity factors, K_I and K_{II}. The energy release rate is defined as

$$G = -\frac{\partial \Pi}{\partial a} \tag{3}$$

which is related to the near-tip field by

$$G = \frac{K_I^2}{E_0} + \frac{K_{II}^2}{E_0} \tag{4}$$

where E_0 is Young's modulus at the crack tip. The energy release rate can be represented by the following line integral:

$$J = \lim_{\Gamma \to 0} \int_\Gamma (W\delta_{1i} - \sigma_{ij}u_{j,1})n_i\, dC \tag{5}$$

where W is the strain energy density and n_i is the outward normal of the path Γ, which starts from a point on the lower crack face and ends at another point on the upper crack face. For the homogeneous case, the integral under the limit is divergence free; therefore, it is path independent and the limit is not needed. In this case, the J in (5) is Rice's J-integral (Rice, 1968). For nonhomogeneous materials, path independence occurs when the crack is perpendicular to the material property variation direction, since in this case the integral is still divergence free.

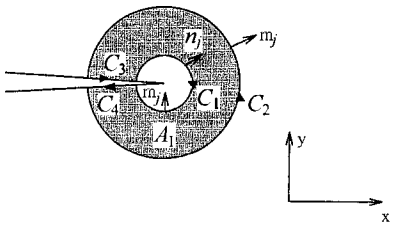

Fig. 1 A simply connected domain A_I enclosed by the contour C ($C = C_1 + C_2 + C_3 + C_4$) near crack tip. The domain is where the domain integral is evaluated.

There are usually several ways to calculate stress intensity factors after the stress and displacement fields are obtained. In the stress matching and displacement matching, the stress intensity factors are obtained by extrapolating from the stresses or displacements ahead of the crack tip using (1) or (2). For example, K_I is obtained by substituting the obtained normal stress ahead of the crack tip into (1). The matching method has the advantage that almost no additional calculation is required even in the FGM case, but it requires a high degree of mesh refinement and often suffers from instability as the crack tip is approached (see Anderson, 1995). Another way, the domain integral method, which is an energy approach based on the J-integral and which has been proved to be efficient for homogeneous materials, is the focus of our numerical study here.

In the domain integral method, the energy release rate J is calculated through an area integral in the two-dimensional case and stress intensity factors are then obtained using (4). The area integral approach provides much better accuracy than directly evaluating the contour integral in (5), and is easier to implement numerically. Early works along the line of the energy approach were given by Parks (1974, 1977), Hellen (1975), and deLorenzi (1982). Shih and his co-workers (see Li, Shih, and Needleman, 1985; Shih, Moran, and Nakamura, 1986; Moran and Shih, 1987) formulated the domain integral methodology in a general way. For homogeneous materials, it has been applied in above works to elastic and plastic material responses, mechanical and thermal loadings, and two-dimensional and three-dimensional spaces. We will discuss the application of the domain integral to nonhomogeneous materials. In particular, we will show that the integral term representing the effect of nonhomogeneity may be neglected when evaluating the integration at a region close the crack tip; therefore, the standard domain integral for homogeneous materials gives sufficient accuracy. We will discuss the elastic case; the conclusion may be extended to the power-law hardening case, i.e., HRR singularity (Hutchinson, 1968; Rice and Rosengren, 1968).

Consider an annular region A_I around the crack tip in the two-dimensional case, as shown in Fig. 1. For simplicity in the discussion, we consider that the material variation is along the x-axis; and only one of the two material parameters, the Young's modulus, has a gradient where the Poisson's ratio is taken as a constant since its variation is usually small compared to the former. The conclusion obtained below can be extended to the general material variation case. Both the inner and outer boundary of the region A_I are sufficiently close to the crack tip. The J given in (5) can be written in terms of the boundary integral,

$$J = \oint_C (\sigma_{ij}u_{i,1} - W\delta_{1j})qm_j ds \tag{6}$$

where $C = C_2 + C_3 + C_1 + C_4$ is the boundary of A_I; m_j is the outward normal of A_I; on C_1, $m_j = -n_j$, and on C_2, $m_j = n_j$; and q is a smooth function which has the value of unity on C_1 and zero on C_2. Applying the divergence theorem to (6) gives

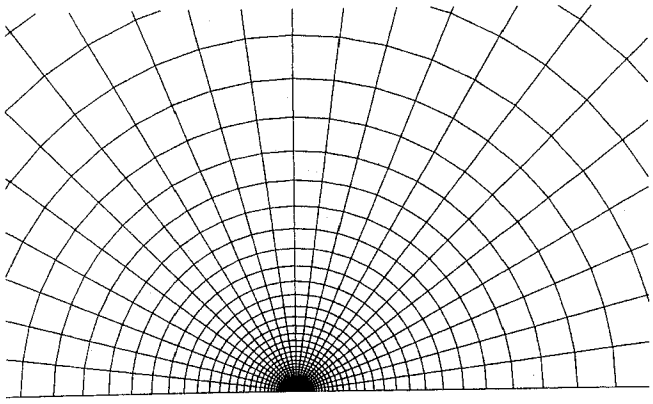

Fig. 2 Finite element mesh of the crack-tip region. In our calculation four-node bilinear elements are used. The smallest element at the tip is 10^{-5} times a characteristic length.

$$J = \int_{A_I} (\sigma_{ij} u_{i,1} - W\delta_{1j}) q_{,j} dA - \int_{A_I} W_{,1} q dA. \tag{7}$$

Here, $W = W[E(x), \epsilon(x, y)]$. The derivative of W under the second integral is with respect to the coordinate x in $E(x)$. Comparing with the homogeneous case, the second integral is an additional term which represents the effect of nonhomogeneity.

In numerical implementation, the inner contour C_1 is usually taken as the crack tip, and the outer boundary C_2 is taken to be the same as element boundaries. The function q defined above is an arbitrary function as long as it gives the correct values at the boundaries, C_1 and C_2. It was shown by Shih and his coworkers in the previously mentioned papers that the calculated J is insensitive to the choice of q. The value of it within an element may be taken as

$$q = \sum_{i=1}^{n} N_i q_i \tag{8}$$

where N_i are the shape functions of the element, n is the number of nodes per element, and q_i are the nodal values of q, which are assigned in accordance with a smooth function varying from zero at the outer boundary to unity at the crack tip. The derivative of q with respect to the coordinate x_i is

$$\frac{\partial q}{\partial x_i} = \sum_{i=1}^{n} \sum_{k=1}^{2} \frac{\partial N_i}{\partial \eta_k} \frac{\partial \eta_k}{\partial x_i} q_i \tag{9}$$

where η_k are the coordinates in the isoparametric space. Evaluating the quantity under the integral in (7) at the Gauss integration points, J is obtained numerically by

$$J = \sum_{A_I} \sum_{p=1}^{n} \left\{ [(\sigma_{ij} u_{i,1} - W\delta_{1j}) q_{,j} - W_{,1} q] \det \left(\frac{\partial x_k}{\partial \eta_k} \right) \right\}_p w_p. \tag{10}$$

Here, w_p is the weight function of integration, and det $(\cdot)$ is the determinant of Jacobian matrix.

The mesh design for our nonhomogeneous problems is a standard mesh design for crack problems. The crack tip is surrounded by an arrangement of wedge-shaped isoparametric elements. The same type of elements makes circular rings which surround the wedge-shaped elements at the tip (see Fig. 2). In this region, the size of the elements increases along the radial direction according to the exponential scale which gives the unit aspect ratio of the elements. The smallest elements at the crack tip are smaller or equal to $10^{-5}a$, where a is a characteristic length. Between the circular region and the region far away from the tip where the stresses vary regularly, there is a transition zone in which the element shape changes gradually from the curved polygon to the regular element shape. The geometry of a typical mesh of this kind was shown in the previously mentioned papers (also see Shih and Asaro, 1989). It is noted that near the tip the mesh needs to be refined to account for the high-stress gradients associated with the singularity; in the FGM case, also to account for the material property variation.

Using this type of mesh, we show here that if we evaluate the domain integral in the region sufficiently small around the crack tip, the value of the second term in (7) involving the derivative of W is very small, essentially negligible. The domain integral in practice can be calculated in the region close to the crack tip (the circular domain consisting of the first 10 or 20 circular rings of elements at the crack tip zone) as demonstrated in the next section. In our calculations, as mentioned above, the smallest element is in the size of $10^{-5}a$, where a is the characteristic length. In such a situation, the second integral in (7) may be estimated as follows. Using the above mesh design, the first 10 or 20 rings of elements are arranged within the radius $10^{-4}a$ from the crack tip. The weight functions for the two integrals in the expression (7) are q and $q_{,j}$. If the pyramid shape for the function q (Fig. 3(*a*)) is used, its derivative with respect to the coordinates is on the order of $10^4 a^{-1}$ considering that the domain is within a circle with radius $10^{-4}a$. Then, the weight functions of the first and second integrals are of the orders 10^4 and 1, respectively. Note that a^{-1} in the derivative of q has been moved to the integrand of the first integral. The first integral is overweighted by its weight function compared to that of the second. On the other hand, the two integrands are not likely to differ by such a large amount as that of the weight functions, i.e., to be of the same order. This is due to the following: (a) they both are essentially energy density terms (energy density unit/length) calculated using stress and strain fields; (b) both are proportional to the loading, the square of the stress intensity factor K_I^2; and (c) the first is proportional to the inverse of the modulus and the second is proportional to the derivative of the modulus divided by the square of the modulus. Since such a small domain for the domain integral is well within the K-dominance zone, the asymptotic expressions (1) and (2) are valid within it. The K-dominance zone for FGMs has been examined in Gu and Asaro (1997b), where it has been shown that within the distance of a few percent of the characteristic length, the difference of the stress fields of the asymptotic and full solutions are within a few percent. Substituting (1) and (2) into the two integrands, (b) and (c) can be confirmed. This permits us to write

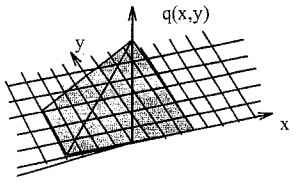

(a) pyramid function

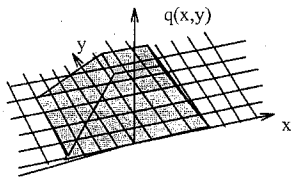

(b) plateau function

Fig. 3 The two often used shapes of q function

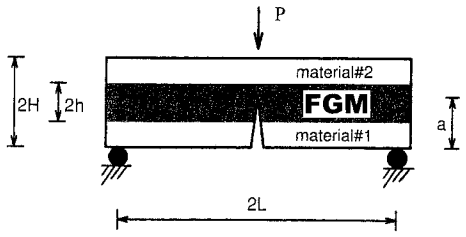

Fig. 4(*a*)

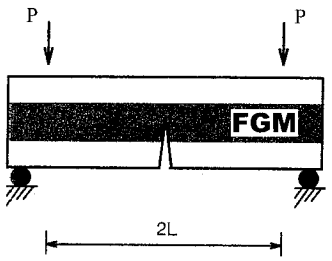

Fig. 4(*b*)

Fig. 4 Two sandwiched bending specimens with FGM interlayer: (*a*) three-point bending; (*b*) four-point bending

$$[\text{first integrand}] = \frac{K_I^2}{E_0 a}\frac{f_1(\theta)}{r}$$

$$[\text{second integrand}] = \frac{K_I^2 E_0'}{E_0^2}\frac{f_2(\theta)}{r}. \qquad (11)$$

In (11), E_0' is the derivative of the Young modulus at the crack tip; f_1 and f_2 are obtained from angular functions in (1) and (2), and therefore they do not have much effect on the magnitudes of the two integrands. In our discussion, we assume that there is only mode I loading. However, one can obtain the same conclusion for mixed-mode presentation through similar steps. Also, $E_0'a$ is roughly proportional to E_0 as can be seen from the following example. Consider the FGM interlayer in Fig. 4 with linear modulus variation, we have $E_0 = (E_2 + E_1)/2$ and $E_0'a = E_0 a\zeta/2/h$ when the crack tip is at the middle of the FGM interlayer, where the subscripts denote the properties for material #1 and #2, and $\zeta = (E_2 - E_1)/(E_2 + E_1)$. The variation of the multiplier ζ, as E_2/E_1 varies, is small. So, the two scale factors in the above expression (11) would not differ much as long as a and h do not differ much, and this is similar for other material variation forms. Note that if h is the smallest length compared to other dimensional lengths, one could chose the characteristic length a to be h so that $a/h = 1$. If E_0 and $E_0'a$ are of the same order, from the above analysis we estimate that the first integral is 10^4 times the second integral. In general, the difference between E_0 and $E_0'a$ is not significant at all, compared to that of the two weight functions and therefore the second term in (7) may be neglected. It may also be shown that the conclusion is true by a similar step if the plateau shape for the q function (Fig. 3(*b*)) is used.

Suppose that r_D is the radius of domain where the domain integral is evaluated and within it the field can be well represented by the singular field (1) and (2), then from the above analysis the error of neglecting the second term can be estimated as

$$e \approx \frac{r_D E_0'/E_0}{1 + r_D E_0'/E_0}. \qquad (12)$$

The error is very small if we choose r_D to be sufficiently small. The simplified method has the following advantages: (a) it gives the same accuracy for the stress intensity factors as the domain integral for homogeneous materials, as we shall see in numerical examples; (b) the input of the derivatives of the material properties (gradients) is not required such that in the numerical implantation only material properties need to be assigned to elements or Gauss integration points and this is easy to achieve; and (c) no additional calculations are required as compared to the homogeneous case.

When the gradient of the thermal expansion coefficient of the FGM does not vanish and thermal loading (temperature change) is applied, the additional term related to the gradient of the thermal expansion coefficient is an integrand under the second integral in (7) which can be written as

$$[\text{thermal term under second integral}] = K_I T_0 \alpha_0' \frac{f_3(\theta)}{\sqrt{r}} \qquad (13)$$

where T_0 is temperature change at the crack tip, α_0' is the gradient of thermal expansion coefficient at the crack tip, and f_3 is obtained from the angular function in (1). This term may also be neglected due to the following reasons. First, it is under the second integral in (7). As analyzed before, the first integral is overweighted. Second, the $1/r$ factor in first integrand, given in (11), is much larger than the $1/\sqrt{r}$ factor in (13), in the domain with radius $10^{-4}a$. Third, since the stress solution only depends on the ratio of the muduli of the two bulk materials for traction problems (as we shall see in next section), the two moduli may be chosen in the calculation such that $1/E_0$ in (11) is in a normal range. Having these, we can estimate that the magnitude of (13) and that of the first expression of (11) do not differ much.

We have gone a rigorous way to show that the standard domain integral can be directly used for nonhomogeneous materials. A simple way to argue this is that since the asymptotic expressions (1) and (2) are the same as those for homogeneous materials with the material properties being those at the crack tip, there exists a small homogeneous zone which may be regarded as the K-dominance zone so that the standard domain integral is valid there. But from this simple way it is impossible to obtain the above error analysis. When the second term is neglected, the expression to numerically calculate domain integral becomes

$$J = \sum_{A_I}\sum_{p=1}^{n}\left\{[(\sigma_{ij}u_{i,1} - W\delta_{1j})q_{,j}]\det\left(\frac{\partial x_k}{\partial \eta_k}\right)\right\}_p w_p, \qquad (14)$$

which is the same as that for the homogeneous case.

When the domain integral is obtained, the stress intensity factors can be evaluated using (4). If there is only mode I stress intensity factor at the tip due to the symmetric material properties, the geometry and the loading, it can be evaluated directly from (4). If it is a mixed-mode problem, the interaction energy release rate defined in Shih and Asaro (1989) may be evaluated instead of the energy release rate in (4). Using the interaction energy release rate, modes I and II can be separated.

3 Numerical Results

We have extensively tested the numerical method using many crack geometries and loadings. The results have been compared with those obtained by other methods, such as displacement-matching and singular integral equations. All showed the method to be accurate, convergent to the correct solution. The domain integral evaluated from the domains near the tip is stable, independent of the domain chosen. The following are four examples that illustrate this.

The first example is an edge-cracked plate made of a FGM, subject to remote constant strain. It has been solved previously by Erdogan and Wu (1993), using the singular integral equation method. We use it to check the accuracy of our scheme. The second and the third are three-point bending and four-point bending specimens made of sandwiched structures with the in-

terlayers being FGMs (Fig. 4). The interlayer is a zone of transition wherein the material properties change smoothly from the upper layer to the lower layer. The length $2L$ is assumed to be sufficiently large so that it would not affect the solutions. The height of the bars is $2H$, the crack length a, and the height of the interlayers $2h$. The crack is perpendicular to the upper and lower boundaries, and its tip is inside the FGM. The sandwiched structures can be used to study either the fracture of FGMs or the interface behavior when the interlayer thickness is small compared to those of the two bulk layers. The geometry of the first example is the same as Fig. 4, and the only difference is that it is a single piece of FGM for the constant strain problem.

The mesh design was discussed in the previous section. The four-node bilinear elements are used in the study. We have extensively tested the numerical method by changing the material properties, the loadings, and the specimen dimensions. We also have changed the size of the domain by changing the number of rings of elements. All of the stress intensity factors evaluated from the domain integral have shown the accuracy of the scheme. The convergence study results will be provided in tabular form later in the section. The material property variation is achieved by using corresponding material properties at Gauss integration points of each element. We use the software package ABAQUS to perform the calculation, and only the user-subroutine UMAT is required for the material variation. The J-integral is also calculated using the standard domain integral function provided in ABAQUS.

For real FGMs, the property variation along the thickness can be linear, exponential, or some other form. For elastic problems, both Young's modulus and Poisson's ratio vary with the position in general. It is assumed in all examples in this section that the former has the major effect and the latter is taken to be constant. It is reasonable to do so since the variation of the Poisson's ratios is usually small compared to that of the moduli. For the problems studied (see Fig. 4), the Young's modulus is expressed by the following:

$$E(y) = Ay + B$$
$$E(y) = A \exp(By) \tag{15}$$

where A and B are material constants which represent material gradients. The origin of the coordinates is at the center of these specimens and y is along the thickness direction. The first expression in (15) is a linear form, whereas the second is an exponential form. Given the moduli of the lower and upper layer, E_1 and E_2, the two constants are expressed as

$$A = \frac{E_2 - E_1}{2h}, \quad B = \frac{E_2 + E_1}{2} \tag{16}$$

for the linear gradient, and

$$A = \sqrt{E_1 E_2}, \quad B = \frac{1}{2h} \log\left(\frac{E_2}{E_1}\right) \tag{17}$$

for the exponential variation.

In the first example, material variation along the thickness is taken to be the exponential form in (15). The loading is a constant strain ϵ_0 far away from the crack at the two ends which gives rise to a remote stress field, $\sigma = \sigma_0 \exp(By)$, where $\sigma_0 = A\epsilon_0/(1 - \nu^2)$. The energy release rate was calculated from the domains formed by the first 20 rings, using the J-integral evaluation function in ABAQUS. The results from the first ten rings are shown in Table 1, given for different E_2/E_1 ratios, and the results from the domains formed by the remaining ten rings of elements basically are the same as those of column 9 and 10 in the table. The ratio E_2/E_1 is the modulus of the upper boundary over that of the lower boundary. In the calculation we choose $\sigma_0 = 1$ and the crack length $a = 1$. From the table, the convergence of the numerical method is clearly seen. When the ratio is 1, it represents homogeneous material. In the strong material variation case, the ratio is 10. We see that in both cases the convergence behavior is the same. So, we may conclude that the convergence of using the standard domain integral for FGMs is the same as that for homogeneous materials. The domain integral scheme has been proved to be a useful one in the numerical analysis of the homogeneous fracture. Note that those results from the domains formed by the first two rings usually have a relatively large error in both the homogeneous and FGM case, due to the inaccuracy of the innermost elements. Thus, those results from the domains formed by the first two rings may be disregarded. The stress intensity factors obtained from the four cases in the table, in which the ratio is equal to 0.1, 0.2, 5, and 10, are 4.01, 4.22, 6.49, and 7.48, respectively. These results are the same as those obtained from the singular integral equation method provided by Erdogan and Wu (1993).

Due to the symmetric geometries and symmetric material properties with respect to the crack line for the two specimens in Fig. 4, there is only mode I stress intensity factor at the crack tip for the second and third examples. Since the near-tip fields are of the same form as those for homogeneous materials, the generic form of the stress intensity factor may be written as

$$K_I = Ta^{1/2} Y\left(\frac{E_2}{E_1}, \frac{a}{H}, \frac{h}{H}, \wp\right) \tag{18}$$

where T is a representative stress magnitude, a is a characteristic length (can be taken as the crack length) and Y is a dimensionless function which is related to the geometries of the problems and material properties: the ratio of the moduli and $\wp$, the form of material variation. There are four independent variables in the dimensionless function Y. For known material variation $\wp$ and the thickness of the FGM h/H, the solution Y depends on the modulus ratio and the position of the crack tip a/H, and may be systemically presented by tables or figures. For example, if using tables, each table contains the solution for given $\wp$ and h/H, where the row represents E_2/E_1 and the column represents a/H. If using figures, each figure contains the solution for given $\wp$ and h/H, and in the figure each curve corresponds to a value E_2/E_1 with the x-axis being a/H. Given the representatives of $\wp$ and h/H, we construct the complete solution in above ways for others to use. For homogeneous materials, Y is only related to a/H. It is obtained in terms of a figure or empirical expressions which are given in the handbook by Tada et al. (1985).

Figure 5 shows the solution of mode I stress intensity factor versus the position of the crack tip in the FGM for linear mate-

Table 1 Convergence for the Remote Constant Strain Problem

	Energy release rate calculated from the first ten rings [in units of $\sigma_0^2 a/E_1$]									
E_2/E_1	1	2	3	4	5	6	7	8	9	10
0.1	42.43	46.15	46.21	46.24	46.25	46.26	46.26	46.26	46.28	46.27
0.2	33.26	36.17	36.22	36.24	36.25	36.26	36.26	36.26	36.27	36.27
1	20.99	22.83	22.86	22.88	22.88	22.89	22.89	22.89	22.90	22.90
5	15.76	17.14	17.16	17.17	17.18	17.18	17.18	17.18	17.19	17.19
10	14.78	16.07	16.09	16.10	16.11	16.11	16.11	16.11	16.12	16.12

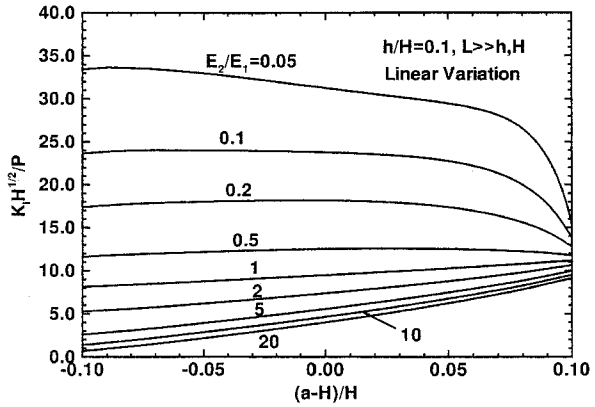

Fig. 5 Stress intensity factor versus crack-tip position in the FGM interlayer for three-point bending with $h/H = 0.1$

rial variation in the three-point bending specimen, where $h/H = 0.1$. The geometry represents the case where the interlayer of FGM is considerably thin compared to the two bulk materials. It is seen that the curves in the figure are the nondimensional function Y in (18) if the characteristic length is taken to be H. The solutions of this kind for various h/H and $\wp$ form a complete solution for the three-point bending specimen. Usually tough materials such as metals have a lower modulus than brittle materials such as ceramics. From this figure, when the crack travels from a tough side (the side with smaller modulus) to a brittle side (the side with larger modulus) the crack-tip stresses increase. The energy release rate calculated from the domains formed by the first ten rings of elements is listed in Table 2 for both linear and exponential material variations. The stable results in the table again show the convergence of the numerical scheme. When the toughness of the two bulk materials is different, it is expected to vary along the thickness of the FGM and can be written as $\Gamma((a - H)/H)$ in the FGM. Then, for stable growth in the FGM interlayer we have

$$G\left(\frac{a-H}{H}\right) = \frac{K_I^2\left(\frac{a-H}{H}\right)}{E\left(\frac{a-H}{H}\right)} = \Gamma\left(\frac{a-H}{H}\right)$$

$$\frac{\partial G\left(\frac{a-H}{H}\right)}{\partial a} < \frac{\partial \Gamma\left(\frac{a-H}{H}\right)}{\partial a}. \qquad (19)$$

For unstable growth, in the second equation "<" is replaced by ">." Let's consider a special case where the toughness is constant across the thickness of the FGM. From the figure, we see in this special case that when material #2 is much softer than material #1, $E_2/E_1 \ll 1$, the crack growth is likely to be stable. This is especially true when the crack tip is close to material #2. When material #2 is stiffer than material #1, the crack growth is likely to be unstable. In general, if the toughness varies with position and the crack is close to material #2 with $E_2/E_1 \ll 1$, it is a stable growth when the decrease of the slope in the figure overcomes the decrease of the toughness. Figure 6 represents the case when $h/H = 0.5$ and other parameters are the same as Fig. 5. From the two figures we see that the trend of these curves has a dramatic change as the percentage of the FGM changes, and this is especially true for those curves with $E_2/E_1 < 1$. For many crack-tip positions in Fig. 6 the stress intensity factor increases as the crack length increases. This means that if the increase of the toughness at the crack tip as the crack length increases is not as fast as the stress intensity factor, it is an unstable growth for the crack tip traveling in those positions. In the above discussion of the crack growth, we have assumed that the crack propagates along the original direction, since these are the cases where geometry, loading, and material are symmetric with respect to the crack line. A first-order approximation model, which is based on local homogeneity, has been used to examine the crack propagating direction for several cracked FGM geometries (Gu and Asaro, 1997b). The model also predicts that a crack grows along its original direction when everything is symmetric.

For the four-point bending specimen shown in Fig. 4, the two ends far away from the crack line is in a pure bending state, where the bending moment $M = Pl$ and l is the distance between the applied force and the support of the beam. The neutral axis changes with material properties, material variation, and layer's thicknesses and is known when these are given. Our numerical results show very good convergence as those listed in Table 1 and 2. Figures 7(a) and (b) illustrate the stress intensity factor versus the interlayer thickness for the crack tip at the center of the beam and linear material variation. It is recognized that these curves are the function Y in (18) if the characteristic length is chosen as H. Compared to Fig. 5, this is another way to present the solution: each curve represents a case for a value E_2/E_1, given $\wp$ and a/H. In these two figures, for a fixed H and as h/H increases, the K_I increases when $E_2/E_1 > 1$ and decreases when $E_2/E_1 < 1$. When h/H is zero, it is the bimaterial solution. The figure tells us that although the increase of the percentage of the FGM in the structure due to the increase of interlayer thickness reduces the mismatch between the two bulk materials, it may not reduce the stress intensities at the crack tip. The increase or decrease of the stress intensities depends on the crack position. As far as the crack propagation is concerned, at this point we do not know how the toughness changes with the FGM percentage increase (note that the increase of the percentage reduces the material gradients). So we do not know if the increase of FGM percentage can prevent the crack growth. However, under the special case that the toughness is constant for FGM, we may conclude that the increase of FGM percentage may not be good to prevent crack growth. In another paper (Dao et al., 1997) we have shown that the increase of FGM percentage may not reduce microstress concentration at the grain size level under thermal loading for a perfect FGM without cracking. The conclusion of the microstress concentration was obtained from a statistically based analysis.

Using a similar analysis, the method can be extended to the three-dimensional case. In three-dimensional space, the domain can be chosen such that its boundary is a tube, which surrounds the crack tip and whose radius of the cross section is sufficiently

Table 2 Convergence for the Three-Point Bending Specimen*

	Energy release rate calculated from the first ten rings [in units of $P^2/(HE_1)$]									
$\wp$	1	2	3	4	5	6	7	8	9	10
linear	466.8	507.7	508.4	508.7	508.8	508.9	508.9	508.9	509.1	509.1
exponential	542.7	590.2	591.1	591.4	591.6	591.6	591.7	591.7	591.9	591.8

* The numerical results in the table are for $h/H = 0.1$, $(a - H)/H = -0.1$ and $E_2/E_1 = 0.1$

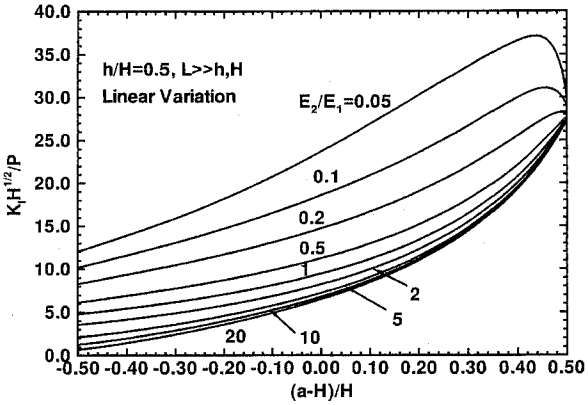

Fig. 6 Stress intensity factor versus crack-tip position in the FGM interlayer for three-point bending with $h/H = 0.5$

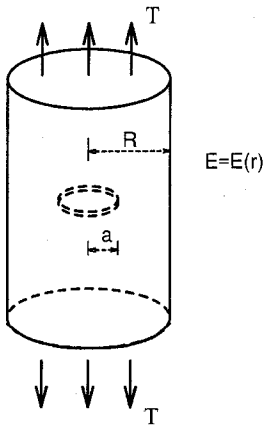

Fig. 8 Penny-shaped crack in a cylindrical FGM solid

small such that the analysis similar to the two-dimensional case can be applied. Detailed discussion of the three-dimensional standard domain integral can be found in previously mentioned papers on the domain integral. The reason for which the simplified method is true is exactly the same as that for the two-dimensional case, i.e., the standard domain integral is overweighted compared to the nonhomogeneous terms. Here we will only give an example of a special version in three-dimensional space, an asymmetric problem shown in Fig. 8. The detailed discussion of the general three-dimensional problem will be given in a separate article elsewhere. The penny-shaped crack (Fig. 8) is in a cylindrical solid. The radius of the crack is a, the radius of the cross section is R, and the length of the solid is so large as not to affect the solution. The Young's modulus is considered to vary along the radius direction, $E = E(r)$. By the structure of the crack-tip field and dimensional consideration, the solution is given in the form

$$K_I = Ta^{1/2}Y\left(\frac{E_2}{E_1}, \frac{a}{R}, \wp\right) \tag{20}$$

where E_2 is the modulus at the outer boundary and E_1 is the modulus at the asymmetric line. The solution to the problem can be easily documented compared to the three-layer bending bars, since we have fewer dependent parameters in the nondimensional function Y here. For given material variation $\wp$, the solution can be presented by a table or a figure. Table 3 shows the convergence for linear and exponential variations, where $E_2/E_1 = 20$ and $a/R = 0.5$. The convergence is very much similar to the two-dimensional case. Except for the first one or two rings, others give the accurate solution.

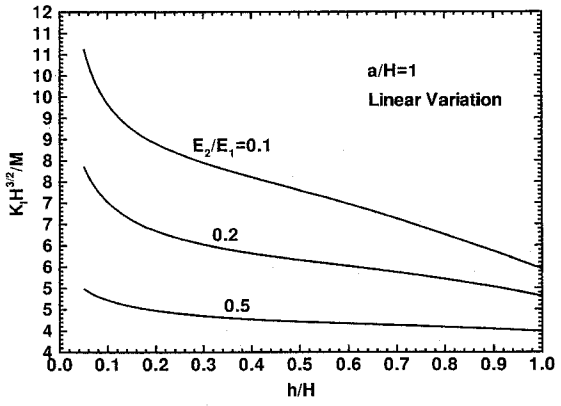

Fig. 7(*a*)

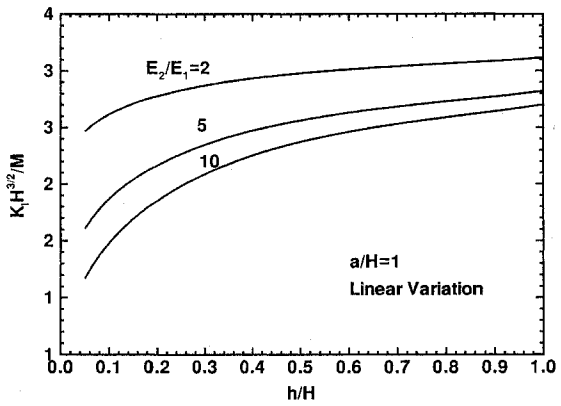

Fig. 7(*b*)

Fig. 7 Stress intensity factor versus thickness of the FGM interlayer for four-point bending

4 Concluding Remarks

We have shown that the standard domain integral can be used to evaluate the crack-tip field for nonhomogeneous materials, such as FGMs. The method requires a sufficiently fine mesh near the crack tip as shown. However, the error induced by the method is estimated such that one can control the error by controlling the size of the domain where the domain integral is evaluated. From the numerical solutions given in the previous section, we have seen that the energy release rate calculated from the domains formed by the rings of elements around the crack tip in this way is very stable and accurate. The examples are all in mode I where both loading, geometry, and material variation are symmetric with respect to the crack face, but the method can be used to calculate the modes I and II stress intensity factors for the mixed-mode case using a defined interaction energy release rate by Shih and Asaro (1989). The method may also be extended to the nonlinear case, such as plastic crack problems. These all suggest that this simplified method, without the input of material gradients and without many changes of the existing finite element code for homogeneous materials, may be well suited for crack mechanics analysis of FGMs where the materials possess gradients. In the examples of the sandwiched structure we have presented the solution in a compact functional form which can be used to easily document a complete solution for other study and design purpose. Finally, it is noted that the material variation is assumed to be continuous across the thickness of the FGM in this study. For real FGMs, the material variation is created by the spatial distribution of one material phase relative to the other. The continuous approach, the proposed numerical method and the fracture behav-

Table 3 Convergence for Penny-Shaped Crack in a Cylindrical Solid*

	Energy release rate calculated from the first ten rings [in units of T^2a/E_1]									
$\wp$	1	2	3	4	5	6	7	8	9	10
linear	0.04260	0.04633	0.04640	0.04642	0.04644	0.04644	0.04645	0.04645	0.04646	0.04646
exponential	0.03286	0.03574	0.03579	0.03581	0.03582	0.03583	0.03583	0.03583	0.03584	0.03584

* The numerical results in the table are for $a/R = 0.5$ and $E_2/E_1 = 20$

ior analysis in the previous section, implies that the particle size of the phases that make the FGMs is very small compared to the crack length and other geometrical lengths, and the microstructure of the FGMs is sufficiently fine. In the above condition, the effect of the particle size in the mechanics analysis may be neglected.

Acknowledgment

This work was supported by the Office of Naval Research through grant N00014-93-1-1164. We are grateful to Prof. C. F. Shih of Brown University with whom we had helpful discussions. We are also grateful to Dr. Q. S. Yu of UCSD who made helpful suggestions in the presentation of the material.

References

Anderson, T. L., 1995, *Fracture Mechanics—Fundamentals and Applications,* 2nd Ed., CRC Press, Boca Raton, FL.

Dao, M., Gu, P., Maewal, A., and Asaro, R. J., 1997, "A Micromechanical Study of Residual Stresses in Functionally Graded Materials," *Acta Metallurgica,* Vol. 45, pp. 3265–3276.

Delale, F., and Erdogan, F., 1983, "The Crack Problem for a Nonhomogeneous Plane," ASME JOURNAL OF APPLIED MECHANICS, Vol. 50, pp. 609–614.

Delale, F., and Erdogan, F., 1988, "On the Mechanical Modeling of the Interfacial Region in Bonded Half-Planes," ASME JOURNAL OF APPLIED MECHANICS, Vol. 55, pp. 317–324.

deLorenzi, H. G., 1982, "On Energy Release Rate and the *J*-Integral for 3-D Crack Configurations," *International Journal of Fracture,* Vol. 19, pp. 183–193.

Erdogan, F., and Wu, B. H., 1993, "Analysis of FGM Specimens for Fracture Toughness Testing," *Ceramic Transactions,* Vol. 34, J. B. Holt et al., eds., The American Ceramic Society, Westerville, OH.

Gu, P., and Asaro, R. J., 1997a, "Cracks in Functionally Graded Materials," *International Journal of Solids and Structures,* Vol. 34, pp. 1–17.

Gu, P., and Asaro, R. J., 1997b, "Crack Deflection in Functionally Graded Materials," *International Journal of Solids and Structures,* Vol. 34, pp. 3085–3098.

Hellen, T. K., 1975, "On The Method of Virtual Crack Extension," *International Journal of Numerical Methods in Engineering,* Vol. 9, pp. 187–207.

Hutchinson, J. W., 1968, "Singular Behavior at the End of a Tensile Crack Tip in a Hardening Material," *Journal of the Mechanics and Physics of Solids,* Vol. 16, pp. 13–31.

Li, F. Z., Shih, C. F., and Needleman, A., 1985, "A Comparison of Methods for Calculating Energy Release Rates," *Engineering Fracture Mechanics,* Vol. 21, pp. 405–421.

Moran, B., and Shih, C. F., 1987, "A General Treatment of Crack Tip Contour Integrals," *International Journal Fracture,* Vol. 35, pp. 295–310.

Parks, D. M., 1974, "A Stiffness Derivative Finite Element Technique for Determination of Crack Tip Stress Intensity Factors," *International Journal Fracture,* Vol. 10, pp. 487–502.

Parks, D. M., 1977, "The Virtual Crack Extension Method for Nonlinear Material Behavior," *Computational Method in Applied Mechanics and Engineering,* Vol. 12, pp. 353–365.

Rice, J. R., 1968, "A Path Independent Integral and The Approximate Analysis of Strain Concentration by Notches and Cracks," ASME JOURNAL OF APPLIED MECHANICS, Vol. 35, pp. 379–386.

Rice, J. R., and Rosengren, G. F., 1968, "Plane Strain Deformation near a Crack Tip in a Power-Law Hardening Material," *Journal of the Mechanics and Physics of Solids,* Vol. 16, pp. 1–12.

Shih, C. F., Moran, B., and Nakamura, T., 1986, "Energy Release Rate along a Three-Dimensional Crack Front in A Thermally Stressed Body," *International Journal Fracture,* Vol. 30, pp. 79–102.

Shih, C. F., and Asaro, R. J., 1989, "Elastic-plastic Analysis of Cracks on Bimaterial Interfaces: Part I—small Scale Yielding," ASME JOURNAL APPLIED MECHANICS, Vol. 55, pp. 299–316.

Tada, H., Paris, P. C., and Irwin, G. R., 1985, *The Stress Analysis of Cracks Handbook,* 2nd Ed., Paris Publications, St. Louis, MO.